A Time-Domain Impedance Probe for Fast Measurements of Electron Plasma Parameters in the Ionosphere

Edmund Spencer, *Member, IEEE*, David Clark, *Student Member, IEEE*, and Sai Krishna Vadepu, *Student Member, IEEE*

***Abstract*— A new time-domain impedance probe is presented in this paper. The new instrument is able to make measurements of absolute electron density and electron-neutral collision frequency in the ionosphere at temporal and spatial resolutions not previously attained. A single measurement is made in 100 μs, which yields an instantaneous spatial resolution of 0.1 m for sounding rocket experiments. A prototype of this instrument was integrated into the payload of a NASA Undergraduate Student Instrument Program sounding rocket launched out of Wallops Island on March 1, 2016. Here, we describe the instrument, and present the data obtained from the sounding rocket experiment. A 6-V amplitude Gaussian derivative excitation was applied to a dipole probe structure, and the current through the probe terminals measured with a balanced active bridge circuit. The time-domain current response was sampled at 5 MS/s, at 12-bit resolution. In the course of the flight, the instrument measured a highly nonlinear response of the plasma because of the large input voltage signal applied. The linear theory cannot explain this response, which obscured interpretation of the data. As a result, we used time- and frequency-domain trend analysis to obtain the variation of electron density over the upleg and downleg of the rocket trajectory. The obtained time and fast Fourier transform trends showed enhanced electron densities in the F layer, which confirmed that the instrument was able to measure the density variations during a significant portion of the flight.**

***Index Terms*— Impedance, instrument, ionosphere, plasma, probe.**

I. Introduction

A PLASMA impedance probe is an instrument that derives the absolute electron density and other plasma parameters by applying a known input voltage, usually sinusoid, across the probe terminals, varying the input frequency, and measuring the current through the probe at each frequency to obtain the impedance of the plasma-probe configuration. The excitation sinusoidal signals are usually kept as small as necessary in amplitude to ensure a linear response while maintaining sufficient signal to noise ratio. The electric current through an electrically short ($L \ll \lambda$) antenna, when driven by a time varying input voltage, depends on the electron density n_e, electron-neutral collision frequency ν_{en}, and the ambient magnetic field $\vec{B}$. At electron scales where the applied excitation frequency ω is close to the electron plasma frequency ω_{pe}, certain resonances can be clearly observed which are proportional to the electron cyclotron frequency Ω_{ce} and the upper hybrid resonance (UHR) ω_{uh}. These two frequencies are related to the absolute electron density n_e through the relations

$$\omega_{uh}^2 = \omega_{pe}^2 + \Omega_{ce}^2 \tag{1}$$

where $\Omega_{ce} = eB_0/m_e$ is the electron cyclotron frequency, and $\omega_{pe} = n_e e^2/m_e\epsilon_0$ is the electron plasma frequency. The electron charge, electron mass, and permittivity of free space are e, m_e, and ϵ_0, respectively. By sweeping through a physically relevant range of frequencies for a particular plasma, the impedance magnitude and phase characteristics can be used to infer n_e and other parameters such as the electron-neutral collision frequency ν.

Sweeping through frequencies is the most robust and accurate method, because of its insensitivity to noise and other interferences. It is commonly used in laboratory environments [1], [2], and this is the method employed on previous sounding rocket experiments [3], [4]. In these instances, the probe is called a sweeping impedance probe (SIP). On the other hand, for satellites flying in low earth orbits, the sweeping method enforces a limit on the spatial resolution of the measurements, because of the orbital velocity of the satellite. Furthermore, as different frequencies are applied, in turn, the sweeping method measures the plasma impedance per sweep over an extended region of plasma, which reduces the accuracy of each sweep.

With this limitation in mind, a different technique was proposed. The impedance measurement could, in principle, be performed using a short time Gaussian derivative voltage excitation, and the current measured as a response to this time-domain excitation. The frequency-domain impedance can then be obtained using the Fourier transforms of the voltage and current. Although this time-domain method would be faster, and more localized, it was expected to be noisier, and capable of triggering nonlinear plasma modes. A prototype of the new

Manuscript received July 3, 2017; revised July 11, 2018; accepted November 18, 2018. Date of publication January 17, 2019; date of current version February 11, 2019. This work was supported by the National Science Foundation CAREER under Grant 1151450. The review of this paper was arranged by Senior Editor S. Portillo. *(Corresponding author: Edmund Spencer.)*

The authors are with the Department of Electrical and Computer Engineering, University of South Alabama, Mobile, AL 36688 USA (e-mail: espencer@southalabama.edu).

Color versions of one or more of the figures in this paper are available online at http://ieeexplore.ieee.org.

Digital Object Identifier 10.1109/TPS.2018.2890336

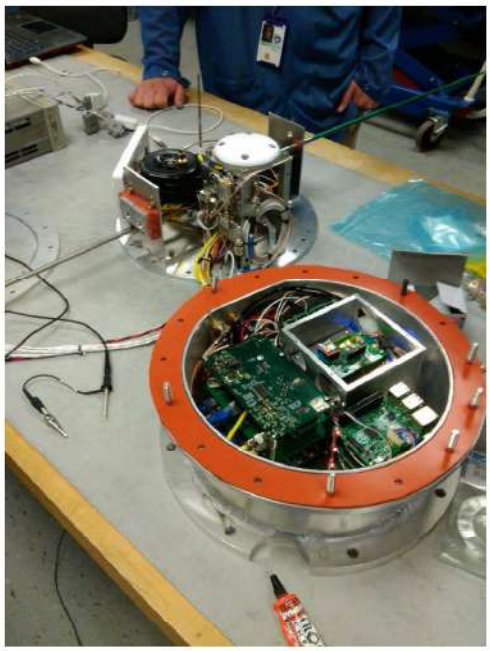

Fig. 1. NASA USIP sounding rocket payload. The TDIP is the visible top board in the electronics stack, shown in the bottom canister. The probe arms are shown extending out of the top canister in the picture.

instrument was, therefore, developed to be flown on a sounding rocket before being adapted for operation on a satellite.

The prototype time-domain impedance probe (TDIP) was integrated into a NASA Undergraduate Student Instrument Program (USIP) sounding rocket payload scheduled for launch out of Wallops Island, as part of a suite of plasma instruments. This is shown in Fig. 1.

In the following, we first describe the instrument in Section II, give a condensed analysis of the expected measurement using the linear theory in Section III, present the results from the USIP sounding rocket experiment and analyze these results in Section IV, and draw some conclusions in Section V. We also discuss future work under way for the next iteration of the instrument.

II. Instrument Description

A SIP uses a frequency sweeping technique in which a sinusoidal stimulus is applied to the probe. The frequency of this sinusoid is then swept from low to high frequencies while the magnitude and phase response are measured. This method requires a sinusoidal generator that is extremely precise in both magnitude and frequency. The new TDIP measures the impedance of a dipole antenna immersed in a plasma by using a shaped, short time pulsed input voltage signal and measuring the current response. This wideband method captures the entire frequency spectrum of interest in a single snapshot, and does not require precise calibration of the pulse source because the input pulse is sampled during each measurement. This is especially useful in satellite missions where measurements of the plasma environment are highly dynamic due to the spacecraft velocity.

A simplified version of the TDIP schematic is shown in Fig. 2. The input into the circuit is a Gaussian derivative

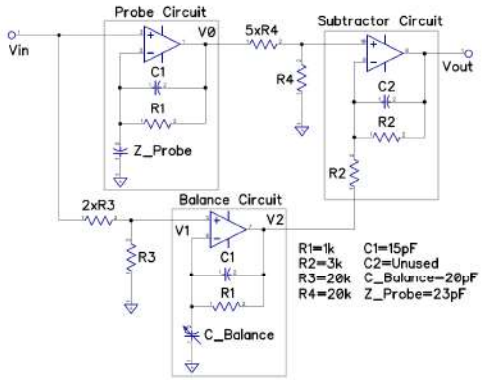

Fig. 2. Analog front-end circuit configuration. The bridge circuit is designed to produce zero output in the absence of a plasma. The impedance Z_Probe shown is equivalent to Z_A in the text. Also, Z_B in the text is related to $1/j\omega$C_Balance.

pulse at terminal V_{in}. This input is fed into two arms of a balanced bridge, the top arm connects to the probe circuit, while the bottom arm is connected to a balance circuit consisting of an adjustable capacitor bank. When no plasma is present the capacitance C_Balance is adjusted until zero output is produced at terminal V_{out}, after a subtractor circuit [5]. When a plasma is present, there will be a difference proportional to the plasma ac current measured at V_{out}. In addition, our circuit incorporated guard traces and a guard drive circuit to reduce the shunt capacitance up to the antenna. Furthermore, a triaxial cable was used to drive the antenna. The inner core was driven in phase with a first outer shield. A second outer shield was grounded.

The input Gaussian was synthesized from a table of values stored in the main processor, and then driven from a 12-bit digital to analog converter sampled at 10 MS/s. The output difference signal voltage was read by a 12-bit analog to digital converter (ADC) sampled at 5 MS/s. The instrument was designed to launch in the night time when upper hybrid frequencies were expected to not exceed 1.8–2 MHz between 80 and 150 km.

The difference signal can be used together with the input voltage and circuit preflight calibration to yield the plasma impedance curve as a function of frequency. When a fast Fourier transform (FFT) of the time-domain error signal between both arms $e(\omega)$ from the instrument measurements are taken, it will be related to the input voltage FFT through the relation

$$e(j\omega) = V(j\omega)Z_f(j\omega)\left[\frac{1}{Z_A(j\omega)} - \frac{1}{Z_B(j\omega)}\right] \tag{2}$$

where Z_f is the matched feedback impedance in the each of the bridge circuit's noninverting amplifier, and Z_B is the impedance on the balance section of the bridge. Inverting this expression gives

$$Z_A(j\omega) = \frac{V(j\omega)Z_B(j\omega)Z_f}{e(j\omega)Z_B(j\omega) + V(j\omega)Z_f(j\omega)}. \tag{3}$$

This expression is used later to analyze the sounding rocket data. Z_B is related to $1/j\omega$C_Balance in the circuit of Fig. 2, while Z_A is the same as Z_Probe in that figure.

III. Theory of the Measurement

In what follows, we give a brief explanation of the expected performance of the instrument using the linear theory of interaction between the plasma and the probe. The theoretical expectation is based on previous success using the sweeping method to perform the measurement of plasma impedance. We discuss the expected resonances that should be observed from the linear theory, and provide an expression for the complete impedance of the plasma-probe configuration. We also give a simple expression for the current waveform expected to be observed in the time domain.

Consider a cold, magnetized, and collisional plasma in the fluid approximation, and further, that the frequency content ω of any excitation of the plasma is much higher than the ion plasma frequency, ω_{pi}, such that ion dynamics can be neglected. Also, since the electron thermal velocities are much higher than the rocket velocity (no more than 6:1 between 100–200 km), we also neglect the spacecraft velocity U_s in this formulation. The dynamical equations for electron motion in the region around the probe are then given as

$$\frac{\partial n_e}{\partial t} + \nabla \cdot (n_e \vec{u_e}) = 0 \tag{4}$$

$$m_e n_e \left(\frac{\partial \vec{u_e}}{\partial t} + (u_e \cdot \vec{\nabla}) \vec{u_e} \right) = -e n_e (\vec{E} + \vec{u_e} \times \vec{B}) - m_e n_e \nu_{en} \vec{u_e} \tag{5}$$

$$\nabla \times \vec{E} = -\frac{\partial \vec{B}}{\partial t} \tag{6}$$

$$\nabla \times \vec{B} = \mu_0 \vec{J_e} + \frac{1}{c^2} \frac{\partial \vec{E}}{\partial t} \tag{7}$$

$$\nabla \cdot \vec{E} = -\frac{e n_e}{\epsilon_0} \tag{8}$$

$$\nabla \cdot \vec{B} = 0 \tag{9}$$

$$\vec{J_e} = -e n_e \vec{u_e} \tag{10}$$

where the first two are the electron continuity and momentum equations, and the remaining are the Maxwell equations.

By virtue of the electron continuity and momentum equations shown earlier, the interaction of the probe and plasma is necessarily nonlinear. If a small amplitude signal is applied to the probe, perturbation theory can be used to linearize the electron equations of motion, and the first-order interaction will produce linear resonances. However, in addition to the amplitude of the perturbations being small, it is also necessary that the spatial gradient of the perturbation signal be small. This depends on the slew rate of the applied signal. The results from the rocket measurements indicate that both requirements may not have been met, the first because our applied signal of 6-V p-p was large, and second that the slew rate of the input Gaussian was perhaps too high. The reason we applied a larger signal than usual is because we anticipated a low signal to noise ratio. The slew rate was high partly because of this. Second, by applying a single pulse containing the entire spectrum of frequencies of interest, as opposed to applying one sinusoid at a time, the total energy input into the plasma was higher. This is a weakness in the time-domain method that needs further investigation if the accuracy of measurements as well as speed of acquisition is to be optimized.

Another significant issue that must be considered in a complete analysis is the fact that a plasma sheath is present around the probe, which creates a static electron and ion density profile extending up to several centimeters out from the probe. In addition, there will be a constant flux of electron or ion current, depending on the payload potential with respect to the surrounding plasma as due to spacecraft charging. These effects can only be understood with a fully nonlinear analysis or simulation.

In any case, if we consider the linearized electron equations of motion, we obtain, after Fourier transformation

$$i\vec{k} \cdot \vec{E} = -\frac{en}{\epsilon_0} \tag{11}$$

$$i\vec{k} \cdot \vec{B} = 0 \tag{12}$$

$$i\vec{k} \times \vec{E} = i\omega \vec{B} \tag{13}$$

$$i\vec{k} \times \vec{B} = \mu_0 \vec{J} \tag{14}$$

$$\vec{J} = -e n_0 \vec{u_e} \tag{15}$$

for the Maxwell equations, and

$$-i\omega n + n_0 (i\vec{k} \cdot \vec{u_e}) = 0 \tag{16}$$

$$-i\omega m_e n_0 \vec{u_e} = -n_0 e \vec{E} - n_0 e \vec{u_e} \times \vec{B_0} \tag{17}$$

for the electron continuity and momentum equations. In this development, the displacement current term in Maxwells equations is neglected, which, therefore, neglects the electromagnetic light waves. Here, we also proceed to neglect the electron-neutral collisions in order to more clearly emphasize the linear resonances. The instrument measures impedance to electron electrostatic modes ($\vec{k} \parallel \vec{E}$), electron electromagnetic modes ($\vec{k} \cdot \vec{E} = 0$) as well as electron plasma modes propagating at arbitrary angles [10]. The dispersion relations governing each of these modes can be obtained through algebraic manipulation of the fourier transformed relations. We treat each case separately in the following.

The electrostatic resonance parallel to $\vec{B_0}$, ($\vec{k} \parallel \vec{E}$), $T_e = 0$, is given as

$$\omega^2 = \omega_{pe}^2. \tag{18}$$

The electrostatic resonance perpendicular to $\vec{B_0}$ ($\vec{k} \parallel \vec{E}$), $T_e = 0$ is the UHR given as

$$\omega^2 = \omega_{pe}^2 + \Omega_{ce}^2. \tag{19}$$

These resonances are emphasized depending on probe orientation parallel or perpendicular to the ambient magnetic field $\vec{B_0}$.

The electromagnetic resonance that is most clearly observable in the impedance curves is the resonance due to the right-hand circularly polarized wave propagating along $\vec{B_0}$. Solving for this particular mode gives

$$\frac{c^2 k_z^2}{\omega^2} = \frac{\omega_{pe}^2}{\omega(\Omega_{ce} - \omega)} \tag{20}$$

which yields a clearly observable resonance trough at $\omega = \Omega_{ce}$,. This is where energy is most effectively coupled into the plasma.

Of the three linear resonances described, the UHR frequency resonance and the cyclotron frequency resonance are the

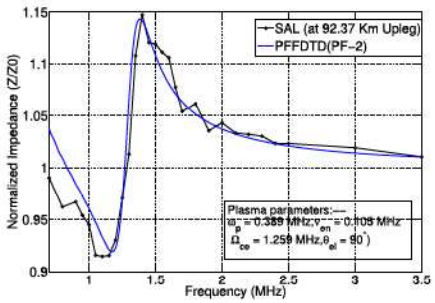

Fig. 3. Data from the SAL sounding rocket using the frequency sweeping technique. The cyclotron resonance f_{ce} can be seen at 1.26 MHz and the UHR f_{uh} can be seen at 1.32 MHz. The impedance from a linear FDTD (PF -FDTD) simulation is fitted to the data.

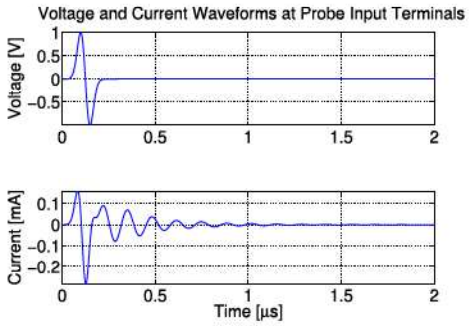

Fig. 4. Applied voltage input into the probe and the expected resultant current at the probe terminals obtained from a full electromagnetic PF-FDTD simulation. The new TDIP attempts to measure this predicted current directly.

most clearly observable. In most instances, identifying these two resonances in the impedance curve gives an immediate estimate of the plasma absolute electron density through (1). In Fig. 3, we show how the cyclotron resonance and UHR appear using the sweeping method to measure impedance on the sudden atom layer (SAL) sounding rocket experiment.

To identify the resonances and determine the collision frequencies accurately, Balmain [8] derived an expression for the impedance of an electrically short dipole immersed in a magnetized plasma. This expression was used in many works devoted to sounding rocket experiments using impedance probes. Ward *et al.* [6] developed a full-wave time-domain electromagnetic code called plasma fluid (PF)-finite difference time domain (FDTD) that simulates the behavior of a short dipole antenna in a magnetized plasma. The code incorporates the linearized electron continuity and momentum equations to model the plasma environment. Spencer *et al.* [7] used the PF-FDTD simulation and the analytical expression in [9] to obtain not only the absolute electron density but also the electron-neutral collision frequencies at selected altitudes for the SAL sounding rocket mission.

The PF-FDTD simulation used a Gaussian derivative pulse excitation to stimulate the plasma resonances in the linear approximation. The input voltage and resulting current response are shown in Fig. 4. This simulated behavior served as the motivation for the time-domain method developed and flown on the NASA USIP experiment that is presented here.

A simplified expression for the current can be obtained through an approximate linear analysis of the plasma-probe interaction. Because the probe dimensions are much smaller than the shortest wavelengths of interest, we can derive the basic behavior by considering a parallel plate capacitive structure immersed in a plasma. The analysis does not include the self-consistent induction field from Faraday's law, but it illuminates the basic behavior. The derivation is given in the Appendix. The current perpendicular to the magnetic field, using Laplace transforms since we wish to show the time domain behavior, is given as

$$I_{\perp}(s) = \left[s + \frac{\omega_{pe}^2 (s+\nu)}{\Omega_{ce}^2 + (s+\nu)^2} \right] C_0 V(s). \tag{21}$$

This is the perpendicular orientation case, that is, when the probe electric field is perpendicular to the ambient magnetic field. If we now calculate the impedance, $Z_{\perp}(s) = V(s)/I_{\perp}(s)$ given as

$$Z_{\perp}(s) = \frac{\Omega_{ce}^2 + (s+\nu)^2}{sC_0[(s+\nu)^2 + (\omega_{pe}^2 + \Omega_{ce}^2)] + C_0 \nu \omega_{pe}^2} \tag{22}$$

we note the appearance of the upper hybrid frequency, $\omega_{uh}^2 = \omega_{pe}^2 + \Omega_{ce}^2$, as a resonance in the impedance when $\nu = 0$. The linear, or small signal, time-domain current response to an arbitrary voltage input is given by the inverse Laplace transform

$$i_{\perp}(t) = \omega_{pe}^2 C_0 V(t) * e^{-\nu t} \cos(\Omega_{ce} t) + C_0 \frac{dV(t)}{dt}. \tag{23}$$

The clearly observable response in the time-domain current is the appearance of the oscillations corresponding to the electron cyclotron resonance, as can be seen in Fig. 4, and the expression above for the current in the time domain. The solution is damped at a rate proportional to the electron-neutral collision frequency, while the plasma frequency is proportional to the square root of the amplitude of the output current. Note that the UHR does not appear explicitly in the expression for the time-domain current, its contribution is embedded in the convolution operation.

IV. Results From NASA USIP Sounding Rocket Experiment

The TDIP was integrated into a NASA sounding rocket launched out of Wallops Island on March 1, 2016, at 8.50 A.M., Eastern Standard Time. Because of the early winter morning launch time, we anticipated some temperature drift in measured values of the input reference Gaussian derivative voltage between the laboratory and during the flight. This did, in fact, appear to be the case. In Figs. 5 and 6, we see the slight difference due to the drifts. In addition, the increased ionization levels in the dawn were expected to yield higher values of electron density compared to a predawn launch. The flight time was approximately 1010 s, from launch to payload impact on the ocean. The rocket reached an apogee of 185 km, flying through the F-layer ionosphere enhanced densities on both the upleg and downleg.

After impact, the payload was successfully recovered and returned in working condition. Some ocean water residue was found on the bottom side of the main board, but this was

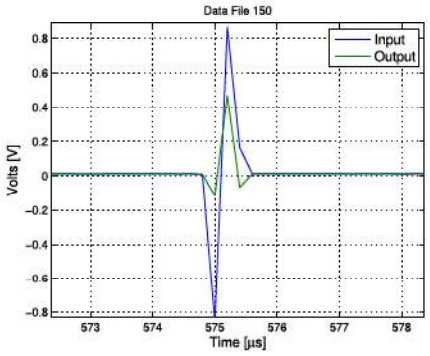

Fig. 5. Measured raw input and output from the instrument after recovery off the coast of Wallops Island. The instrument worked correctly, indicating that there was no electronics malfunction or failure during the flight.

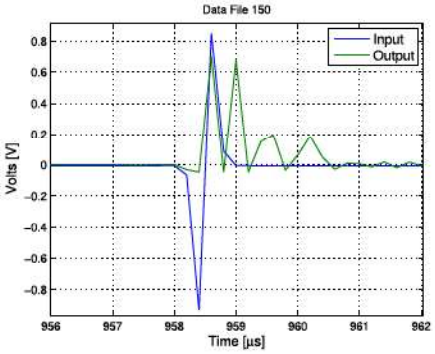

Fig. 6. Sample measurement of output error from the TDIP during the USIP flight. The output current appeared to be rectified or saturated when going negative and was offset by about 0.5 V.

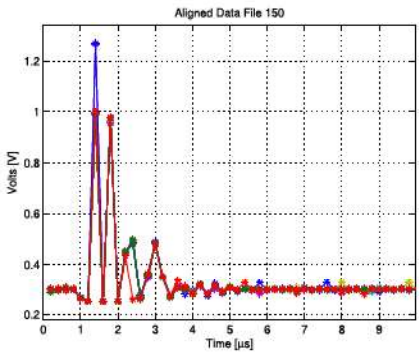

Fig. 7. Superposed output voltages from a single data file (file 150) during the flight. 17 waveforms are superposed in this example. Only one waveform was different from the others.

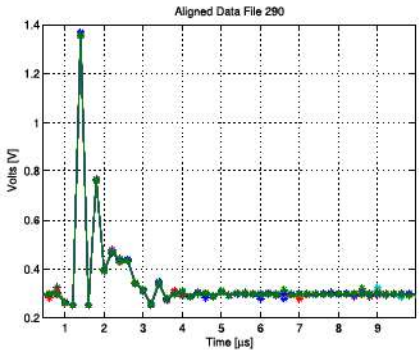

Fig. 8. Superposed output voltages from a single data file (file 290) during the flight. 17 waveforms are superposed in this example. The difference in qualitative features and in the amplitude of the maximum in comparison to the plot in Fig. 7 is clear.

removed through a 90% alcohol bath process. We were able to test the instrument in the laboratory postflight to ensure that it operated correctly. The postflight tests showed the instrument performance to be identical to preflight behavior. Thus, there was no electronics malfunction or failure during the flight.

In Fig. 5, we show the input and error signals as measured in laboratory conditions, with a slightly unbalanced bridge. Because of the difference in capacitance between the probe and balance sections, we see the differentiated input signal appear as an error.

In Fig. 6, the measured response due to a Gaussian input pulse is shown. The input pulses were triggered once every 100 μs, as long as an enable signal was present from the main payload processor to the TDIP. Through the flight, the TDIP generated around 8500 pulses that were stored in 500 data files, each file consisting of 17 pulses or equivalently, 1.7 ms of data sampled at 5 MS/s. The changes in a single file of data were found to be insignificant. Since the rocket moved at a maximum of 1341.5 m/s during the instrument deployment phase, each file contained data equivalent to 2.28-m spatial resolution. This distance is short compared to the scale of altitude dependent density irregularities in the E and F regions. The first 35 files were corrupted and we obtained 475 files of usable data.

In Figs. 7 and 8, we show the measured voltages at two points during the flight. Each plot shows superposed measurements resulting from 17 or 18 pulses. As can be seen, the qualitative features of each set are quite different, between points 5 and 20 on the x-axis. The samples are 0.2 μs apart. However, the measurements made over one file are roughly the same, showing that the results were repeatable. The signal-to-noise ratio as measured was about 50-dB worst case.

It is clear from Figs. 7 and 8 that the measured response did not correspond to the expected response obtained from the linear theory or the PF-FDTD simulations. First, there was an offset due to spacecraft charging of roughly 0.5 V at the ADC inputs. Second, the negative part of the signal appears to saturate. This was across all files. This nonlinear response may be due to a phenomenon called sheath rectification, and can only be analyzed with a fully nonlinear simulation. In the next iteration of the instrument, the size of the input signal needs to be adjustable while in flight, and an offset added to prevent saturation.

We performed a trend analysis of different points on each sampled curve over the entire flight. In Fig. 9, the maximum of each sampled curve is tracked across the 475 data files corresponding to 200 s of measurement time. This maximum occurs at the seventh point on each sampled curve, as can be observed from Figs. 7 or 8. From (23), the initial amplitude of the current is modulated by ω_{pe}^2, this suggested that we track the behavior of the first maximum. We observed that the maximum increased in value during the flight on the upleg, and then decreased on the downleg, with some exceptions. There is

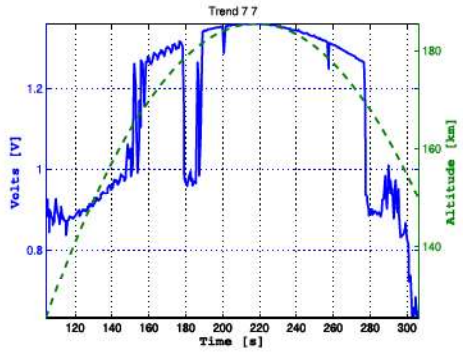

Fig. 9. Trend of point number 7, the first maximum of the output, over the entire flight. 200 s of data consisting of 475 different files, each with about 17 or 18 pulses, were analyzed to produce this trend. The altitude of the rocket with time is also shown.

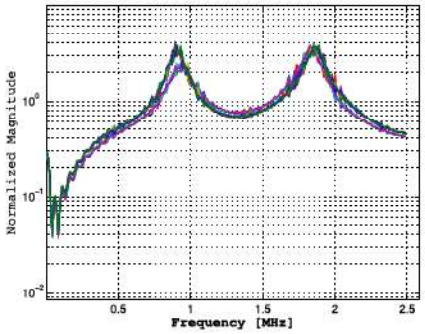

Fig. 10. FFT of the normalized impedance waveform obtained through (3), for the 17 waveforms sampled in file 150. The two peaks at 900 kHz and 1.85 Mhz are used to perform a trend analysis across all 500 files.

a sharp dropout in the data occurring between 175 and 185 s after launch. The reason for this dropout is unclear. There is also a jump in the maximum at about 150 s into the measurements, followed by a similar drop at about 273 s into the measurements. This shows that the maximum became prominent approximately when the payload entered a higher density region in the ionosphere F layer. Below this density, the instrument appeared to be less effective. The altitude with respect to time of the rocket is also shown in this figure, which shows that the sharp rise and fall in the amplitude of the maximum point occurs around 165–170 km on both the upleg and downleg of the flight.

In Fig. 10, the fast fourier transform of the impedance $Z(\omega)$ derived from the error signals in file 150 using the expression in (3) are shown. It is clear that the frequency content is markedly different from those expected using the linear theory. Two peaks appear at 900 kHz and 1.85 MHz. These peaks and the shape of the curve do not correspond to the linear behavior. As a result, we were unable to perform the usual frequency-domain analysis of the waveforms over the flight to infer the electron densities, using linear formulas or the linear PF-FDTD simulations. Instead, we performed a trend analysis by observing the movement of the two frequency peaks over the course of the flight.

The results of the FFT trend analysis are shown in Figs. 11 and 12. In Fig. 11, the trend shows the peak moving upward and then downward in frequency between

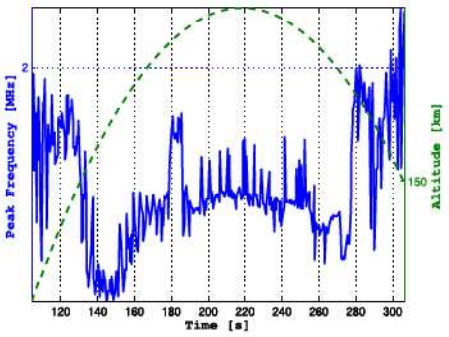

Fig. 11. FFT trend of the bottom peak at 900 kHz, over 500 files (200 s) through the flight. The trend correlates with the trend of the maximum shown in Fig. 9.

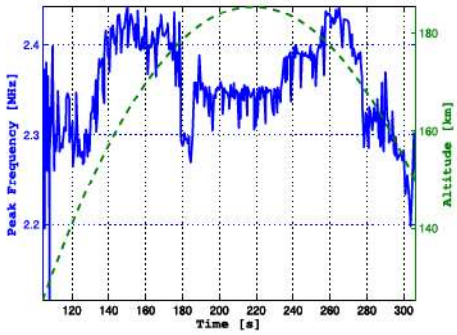

Fig. 12. FFT trend of the top peak at 1.85 MHz, over 500 files (200 s) through the flight. The trend is anticorrelated with the trend of the maximum shown in Fig. 9.

150 and 273 s into the flight. This trend shows the same behavior as the single point maximum trend shown earlier. The same behavior is observed for the upper peak of Fig. 12, except it is anticorrelated with the density increase, as opposed to the earlier two trends.

Before 150 s, the rocket was below about 165 km, and after 273 s, the rocket was below 170 km. The measured results at the altitudes below this level are rising with increasing altitude corresponding to an expected increase of density on the upleg, and falling with decreasing altitude corresponding to an expected decrease of density on the downleg. However, the profiles are qualitatively different between the upleg and downleg portions. This is not surprising since there was a 23-km horizontal distance between the upleg and downleg at the two points occurring at 150 and 273 s, the trajectory being parabolic. We should expect differences in measurements that are further apart horizontally. The correspondence between upleg and downleg is closer as the rocket approaches its apogee, which is also expected. On the other hand, the sudden jump in the measurements occurring at 165 km is not clearly understood.

The anomalies at the altitudes corresponding to 150, 180, and 270 s appear to be connected to the payload related arcing, or sudden changes in payload attitude or interference from other instruments.

V. Conclusion

We have described a new impedance probe for space plasmas that utilizes a time-domain method as opposed to

frequency sweeping methods currently used. The time-domain method appears to be favorable for making measurements with fast moving small satellites in low earth orbit, and the method is shown here to be essentially correct. However, significant challenges remain in deciphering and interpreting the data. This needs theoretical and simulation works that include the nonlinear regime. However, we observed a clear trend in the data which confirms that the instrument measured changes in the ionospheric density with increasing and decreasing altitude that corresponds qualitatively with expected ionospheric density profiles. The observed trends were apparent in both the time and frequency domains, first in the movement of the maximum point in the time signal as the rocket traveled up and then down through the F layer, and second through two clearly observable peaks in the frequency domain that displayed similar behavior. In the second case, the lower peak in the FFT trend was positively correlated with the time-domain trend, while the upper peak was anticorrelated with the time-domain trend. However, the qualitative features were similar above 165-km altitude, closer to where the rocket approached its apogee at 185 km. This result also confirms that the electronics of the new instrument worked correctly throughout the flight, although the probe did not function in the same way during the flight as it did in the laboratory. The next iteration of this instrument is being developed for a cubesat to perform the same measurements at 500-km altitude, where the densities are high, and where the collisional effect is low. The technique will be improved through ensuring that an offset dc voltage can be applied to correct for sheath errors, and the signal amplitude made adjustable to avoid triggering nonlinear behavior.

Appendix
Linear Time-Domain Expression for Current in the Probe

We start with the linearized continuity and momentum equations, and take Laplace transforms in time, with zero initial conditions to obtain a relationship between the electron velocity $\vec{u}_e$ and the electric field $\vec{E}$, and replace the expression for $\vec{u}_e$ into the expression for $\vec{J}_e$, to obtain

$$\vec{J}_e = \frac{\epsilon_0 \omega_{pe}^2}{D(s)} \mathbf{K} \cdot \vec{E} \tag{24}$$

where $\mathbf{K}$ is a tensor given as

$$\mathbf{K} = \begin{bmatrix} \alpha^2+\Omega_x^2 & -\alpha\Omega_z+\Omega_x\Omega_y & \alpha\Omega_y+\Omega_z\Omega_x \\ \alpha\Omega_z+\Omega_x\Omega_y & \alpha^2+\Omega_y^2 & -\alpha\Omega_x+\Omega_y\Omega_z \\ -\alpha\Omega_y+\Omega_z\Omega_x & \alpha\Omega_x+\Omega_y\Omega_z & \alpha^2+\Omega_z^2 \end{bmatrix} \tag{25}$$

and $\alpha = a(s) = s + \nu$. The function $D(s)$ is given by $D(s) = a(a^2 + \Omega_{ce}^2)$. In the above-mentioned matrix, we use abbreviated notations for the component specific cyclotron frequency, that is, $\Omega_x = eB_{ex}/m_e, \Omega_y = eB_{ey}/m_e$, and $\Omega_z = eB_{ez}/m_e$. The electron charge is $e = 1.6 \times 10^{-19}$ and the electron mass is $m_e = 9.11 \times 10^{-31}$. The electron cyclotron frequency is given by $\Omega_{ce} = eB_e/m_e$ where $B^2 = B_x^2 + B_y^2 + B_z^2$. In the above-mentioned relationship, the earth's magnetic field is used, $\vec{B}_e = B_{ex}\hat{x} + B_{ey}\hat{y} + B_{ez}\hat{z}$.

A. Parallel Plate Probe With Zero Ambient Magnetic Field

In the case of zero ambient magnetic field, the tensor $\mathbf{K}$ reduces to a scalar, and the electron current density $\vec{J}_e$ becomes

$$\vec{J}_{e||} = \frac{\epsilon_0 \omega_{pe}^2}{\alpha} \vec{E}. \tag{26}$$

We use this relation as follows. For a capacitive parallel plate probe with plasma confined between the plates, we can use the standard approach of finding a relative permittivity for the plasma between the plates. To get the equivalent capacitance using two capacitor plates and plasma between plates, we restrict the electric field lines to exist only between the plates. We further assume that the electric field is normal to the surface of the plates. The current into the plates J_{in} will equal the plasma electron current added to the displacement current between the plates, $J_{\text{wire}} = J_e + J_D$, where J_e is the electron current due to charge motion, while J_D is the displacement current, or capacitive effect. Implicitly, we are making the following approximation that the electric field is only due to the imposed excitation and that we can neglect the contribution from the changing magnetic field between the plates, effectively neglecting the inductive effect from Faradays law. This results in

$$J_{in} = \epsilon_0 \left[1 + \frac{\omega_{pe}^2}{s(s+\nu)} \right] sE. \tag{27}$$

Integrating over the capacitor plate surface A and letting $E = V/d$, we obtain

$$I_{||}(s) = \left[1 + \frac{\omega_{pe}^2}{s(s+\nu)} \right] sC_0 V(s) \tag{28}$$

where $C_0 = \epsilon_0\ A/d$ is the effectie free space capacitance of the probe structure. The impedance is then given as

$$Z_{||}(s) = \frac{s+\nu}{C_0\left(s^2 + \nu s + \omega_{pe}^2\right)}. \tag{29}$$

In the frequency domain (when $s = j\omega$), the impedance will exhibit a resonance at $\omega = \omega_{pe}$. The time-domain current response to an arbitrary voltage input with $v(t = 0) = 0$ will bc

$$i_{||}(t) = C_0 \frac{dV(t)}{dt} + \omega_{pe}^2 C_0 e^{-\nu t} * V(t). \tag{30}$$

B. Parallel Plate Probe With Ambient Magnetic Field

In this case, we let $\vec{B}_e = B_0\hat{(z)}$. If the plates surfaces are perpendicular to the z-axis and the electric field is taken to be parallel to $\vec{B}_e$, then the resulting expressions degenerate to the case with no magnetic field. The diametrically opposite case is with the plate surfaces parallel to the z-axis and the electric field perpendicular to the plates, and confined to the plasma volume between the plates. In this case, we can reorient the axes to get only $\vec{E}_x$, and the tensor $\mathbf{K}$ reduces to

$$\mathbf{K} = \begin{bmatrix} \alpha^2 & -\alpha\Omega_z & 0 \\ \alpha\Omega_z & \alpha^2 & 0 \\ 0 & 0 & \alpha^2+\Omega_z^2 \end{bmatrix}. \tag{31}$$

With this simplification, we obtain the current through the probe in a manner similar to the procedure above, and obtain

$$I_{\perp}(s) = \left[s + \frac{\omega_{pe}^2 (s+\nu)}{\Omega_{ce}^2 + (s+\nu)^2} \right] C_0 V(s). \tag{32}$$

This is the perpendicular orientation case, that is, where the probe electric field is perpendicular to the ambient magnetic field. We note the appearance of the upper hybrid frequency, $\omega_{uh}^2 = \omega_{pe}^2 + \Omega_{ce}^2$, as a resonance in the impedance when $\nu = 0$, where $Z_{\perp}(s)$ is given as

$$Z_{\perp}(s) = \frac{\Omega_{ce}^2 + (s+\nu)^2}{sC_0\left[(s+\nu)^2 + \left(\omega_{pe}^2 + \Omega_{ce}^2\right)\right] + C_0 \nu \omega_{pe}^2}. \tag{33}$$

The time-domain current response to an arbitrary voltage input is

$$i_{\perp}(t) = \omega_{pe}^2 C_0 V(t) * e^{-\nu t} \cos(\Omega_{ce} t) + C_0 \frac{dV(t)}{dt}. \tag{34}$$

We do not present an expression for the impedance or the current for an arbitrary magnetic field orientation with respect to the plates. It turns out to be more beneficial to obtain a general formula for the impedance of a probe structure possessing any dipolar field structure, as long as inductive effects are neglected and no radiation is present. It should be noted that in the current approximation, the derived expressions are obtained from consideration of the component of the current density parallel to the electric field.

ACKNOWLEDGMENT

The authors would like to thank Dr. D. Vassiliadis at West Virginia University for flying the instrument on his NASA USIP sounding rocket mission. They would also like to thank NASA Wallops Flight Facility scientists and engineers for their support.

REFERENCES

[1] D. D. Blackwell, D. N. Walker, S. J. Messer, and W. E. Amatucci, "Characteristics of the plasma impedance probe with constant bias," *Phys. Plasmas*, vol. 12, no. 9, pp. 093510, 2005.

[2] D. D. Blackwell, D. N. Walker, and W. E. Amatucci, "Measurement of absolute electron density with a plasma impedance probe," *Rev. Sci. Instrum.*, vol. 76, no. 2, pp. 023503, 2005.

[3] A. Barjatya and C. M. Swenson, "Observations of triboelectric charging effects on Langmuir-type probes in dusty plasma," *J. Geophys. Res.*, vol. 111, no. A10, 2006. doi: 10.1029/2006JA011806.

[4] E. Spencer and S. Patra, "Ionosphere plasma electron parameters from radio frequency sweeping impedance probe measurements," *Radio Sci.*, vol. 50, no. 9, pp. 853–865, 2015 doi: 10.1002/2015RS005697.

[5] T. Suzuki *et al.*, "Sheath capacitance observed by impedance probes onboard sounding rockets: Its application to ionospheric plasma diagnostics," *Earth, Planets Space*, vol. 62, no. 7, p. 579, 2010, doi: 10.5047/eps.2010.01.003.

[6] J. Ward, C. Swenson, and C. Furse, "The impedance of a short dipole antenna in a magnetized plasma via a finite difference time domain model," *IEEE Trans. Antennas Propag.*," vol. 53, no. 8, pp. 2711–2718, Aug. 2005.

[7] E. Spencer, S. Patra, T. Andriyas, C. Swenson, J. Ward, and A. Barjatya, "Electron density and electron neutral collision frequency in the ionosphere using plasma impedance probe measurements," *J. Geophys. Res.*, vol. 113, p. A09305, 2008, doi: 10.1029/2007JA013004.

[8] K. Balmain, "The impedance of a short dipole antenna in a magnetoplasma," *IEEE Trans. Antennas Propag.*, vol. AP-12, no. 5, pp. 605–617, Sep. 1964.

[9] K. Balmain, "Dipole admittance for magnetoplasma diagnostics," *IEEE Trans. Antennas Propag.*, vol. 17, no. 3, pp. 389–392, May 1969.

[10] J. A. Bittencourt, *Fundamentals of Plasma Physics*, 3rd ed. New York, NY, USA: Springer-Verlag, 2004.

Edmund Spencer (M'06) is currently an Associate Professor with the Electrical and Computer Engineering Department, University of South Alabama, Mobile, AL, USA.

His current research interests include space plasma physics, electromagnetics, space science instrumentation, and engineering in the space environment.

David Clark, photograph and biography not available at the time of publication.

Sai Krishna Vadepu, photograph and biography not available at the time of publication.